Successive Multilayer Formation of Cyclolinear Polyorganosiloxanes Floating at the Air−Water Interface. A Synchrotron X-ray Reflectivity Investigation

T. R. Jensen,*,† K. Kjaer,‡ G. Brezesinski,§ J. Ruiz-Garcia,§,⊥ H. Möhwald,§ N. N. Makarova,# and Yu. K. Godovsky^

Interdisciplinary Nanoscience Center, Department of Chemistry, University of Aarhus, DK-8000 Århus C, Denmark; Materials Research Department, Risø National Laboratory, DK-4000 Roskilde, Denmark; Max-Planck Institute of Colloids and Interfaces, Am Mühlenberg 1, D-14476 Golm/Potsdam, Germany; Instituto de Física, Universidad Autónoma de San Luis Potosi, Alvaro Obregón 64, S.L.P. 78000, México; Nesmeyanov Institute of Elementoorganic Compounds, Russian Academy of Sciences, Vavilov str. 28, Moscow 117813, Russia; and Karpov Institute of Physical Chemistry, Ul. Vorontsovo Pole 10, Moscow 105064, Russia

Received April 14, 2003; Revised Manuscript Received June 27, 2003

ABSTRACT: Siloxane polymers self-organized into nanostructures with controllable distinct thicknesses from 1 to at least 6 molecular layers, i.e., 1−6 nm, are investigated. Macroscopic manipulation of the surface pressure for these ultrathin films leads to an architecture with a distinct layer thickness and a highly ordered structure as demonstrated by synchrotron X-ray reflectivity measurements performed in situ at the air/water interface. An atactic polymer of cyclolinear methylphenylsiloxane (CL-PMPhSi) that consists of monomer rings formed by six silicon atoms joined by oxygen is investigated in this study. Surface pressure (π) vs surface area (A) isotherm data for these polymers show up to seven plateaus, and this had been assumed to indicate the formation of multilayers with distinct layer thicknesses consisting of 1, 2, 3, etc. layers. The aim of this work was to prove that such successive multilayers are indeed formed and to study their structure. The high-resolution X-ray reflectivity data ($0.01 < q_z < 0.85$ Å^{-1}) measured with a liquid surface diffractometer allow a detailed structural analysis using both a model-independent method and slabs as a layer model. The extracted electron density profiles in the direction of the surface normal are in good correspondence with calculated profiles based on the crystallographic structural analysis of the bulk crystalline monomer. The layered structure of the thin film is clearly visible in the electron density profiles.

1. Introduction

Self-organization of macromolecules into novel highly ordered architectures by noncovalent interaction plays a crucial role within nanoscience, offering the potential of, e.g., exploring storage of information or functional materials for a variety of applications.[1−3] Thin films of organosiloxanes are investigated intensively due to a number of potential applications, e.g., as biocompatible coatings and optical or electronical components, as such films are generally chemically and physiologically inert, insoluble, and thermally stable.[4−6] Control and manipulation of layer thickness and structural features on the molecular level in ultrathin films are of vital importance for optimization of chemical and physical properties and rational design of novel improved materials.

A monomolecular layer floating on a liquid/air interface can undergo phase transitions between phases with well-defined two-dimensional crystal structures as a function of surface pressure and temperature.[7] At elevated surface pressures a monomolecular layer is a metastable phase and has a tendency to collapse forming disordered agglomerates or crystallites with three-dimensional structural order.[8] In rare cases monolayers at the air−water interface can undergo stepwise collapse through a series of distinct phases. An unusual collapse process is found for some cyclolinear polysiloxanes having surface pressure−area (π−A) isotherms with up to seven plateaus.[9] The plateaus occur at ratios of the area consistent with a stepwise layer growth from monolayer to bilayer, bilayer to trilayer, etc. The successive multilayer transitions for these materials are a consequence of the mesophase behavior in the bulk and depend on the nature of the substituents at silicon atoms and other molecular parameters.[10,11] However, only limited knowledge on the mechanism of the formation of these phases and their detailed molecular structures is available.

Thin films of siloxane materials have previously been investigated by macroscopic methods at the air/water interface, i.e., by isotherm measurements and Brewster angle microscopy (BAM), but also on a molecular scale by scanning force microscopy (SFM) and X-ray reflectivity on samples transferred to a solid support.[12−15] Surface-sensitive synchrotron X-ray scattering using a liquid surface diffractometer is a powerful method for nanoscale and angstrom scale structural information that can be performed in situ at the air−water interface.[16] The high photon flux from synchrotron X-ray sources enables structural studies of the limited amount of material present in a monomolecular layer or a thin film composed of just a few molecular layers assembled at the air/liquid interface.[17] This approach has been successfully applied for structural investigations of a

† University of Aarhus.
‡ Risø National Laboratory.
§ Max-Planck Institute of Colloids and Interfaces.
⊥ Universidad Autónoma de San Luis Potosi.
Russian Academy of Sciences.
^ Karpov Institute of Physical Chemistry.
* Corresponding author: phone +45 8942 3894; Fax +45 8619 6199; e-mail trj@chem.au.dk.

10.1021/ma034473c CCC: $25.00
Published on Web 08/26/2003

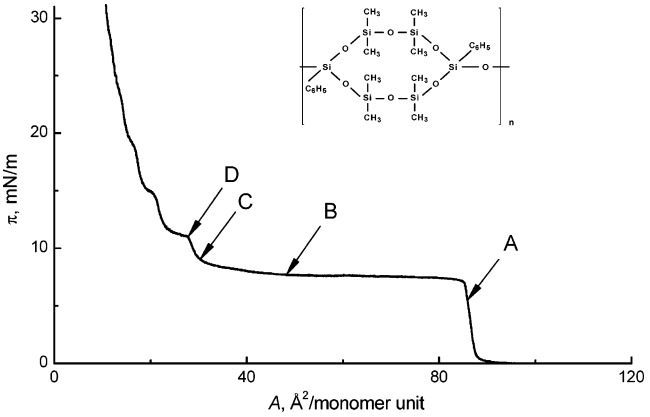

Figure 1. Surface pressure−surface area isotherm of the investigated cyclolinear polyorganosiloxane, CL-PMPhSi. The molecular structure of the monomer consisting of a ring formed by six silicon atoms joined by oxygen and with methyl and phenyl substitutes is shown as an inset. Arrows indicate the values of surface pressure at which the XR measurements were performed: A ($\pi = 5.1$ mN/m), B ($\pi = 7.7$ mN/m), C ($\pi = 9.0$ mN/m), and D ($\pi = 11$ mN/m).

variety of thin films at the air/water interfaces, e.g., self-assembled macromolecules with electronic properties or advanced hybrid organic/inorganic materials.[18,19]

In this work in situ surface sensitive synchrotron X-ray scattering is utilized to gain insight into the fascinating behavior of cyclolinear polysiloxanes at the air/water interface. We focus on the detailed molecular structure of mono- and multilayer thin films and demonstrate a powerful method for polymer science.

Materials and Methods

Materials. We have studied a polymer that consists of monomer rings formed by six silicon atoms joined by oxygen and with two phenyls at the silesquioxane silicon atoms, i.e., atactic cyclolinear poly(methylphenylsiloxane), abbreviated CL-PMPhSi. The chemical structure of the monomer is illustrated in Figure 1 (inset).

The polymer was synthesized by heterofunctional polycondensation of monomers as described below. The monomers 2,8-dichloro-2,8-diphenyl-4,4,6,6,10,10,12,12-octamethylcyclohexasiloxane (**I**) and 2,8-dihydroxy-2,8-diphenyl-4,4,6,6,10,10,12,12-decamethylcyclohexasiloxane (**II**) were prepared according to the procedure described previously but without separation of the isomers.[20−23] Monomers **I** and **II** were characterized by X-ray diffraction and ^{1}H NMR.[24] The molecular weight of the monomer (the repeat unit of the polymer) was $M_m = 555.0$ g/mol, and the length estimated using a Stuart model was $L_m = 9.5 \pm 0.5$ Å.

Poly[oxy(diphenyloctamethylcyclohexasiloxane-2,8-diyl)] (CL-PMPhSi) was prepared according to the procedure described in ref 22. A solution of **II** (1.43 g, 2.50 mmol) and pyridine (0.42 g, 5.0 mmol) in 3.5 mL of dry diethyl ether was added to 1.52 g (2.50 mmol) of **I** in 3.0 mL of dry diethyl ether under an argon atmosphere for 0.5 h. The temperature of the reaction mixture was increased to 70 °C after addition of 2.5 mL of benzene. Benzene (50 mL) was added to the product of the reaction, and C_5H_5N·HCl was separated off; the benzene solution was washed with water and dried under Na_2SO_4. CL-PMPhSi (1.30 g, 48.0%) with viscosity $\eta = 0.49$ dL/g, $M_w = 7.5 \times 10^4$ g/mol, $M_w/M_n = 2.05$ was obtained. The polymer of CL-PMPhSi has the atactic structure where the phenyl rings are randomly oriented. Although the atactic polymer is unable to crystallize, nevertheless, it is mesomorphic with isotropization temperature, $T_i = 415$ °C. The average degree of polymerization, given as the number of monomers per polymer, is $x_w \approx 135$, giving an average length of the polymer, $L_p \approx 128$ nm. Further details on the synthesis can be found in ref 25.

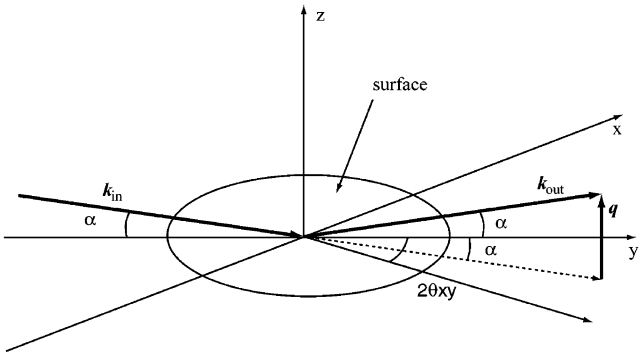

Figure 2. Geometry for X-ray reflectivity measurements. The thin film at the air/liquid interface is shown in the *xy*-plane with the $2\theta_{xy}$ arc. The incident and scattered X-rays are shown as wave vectors, $\mathbf{k}_{in}$ and $\mathbf{k}_{out}$, and the scattering process is characterized by $q_z = \mathbf{k}_{out} - \mathbf{k}_{in}$.[16]

CL-PMPhSi dissolved in chloroform (0.2−0.7 mg/mL) was spread on the water surface, and after evaporation of the solvent the film was compressed slowly to an area corresponding to a monolayer and the pressure was kept constant during data acquisition. Several X-ray experiments could be performed on each sample, allowing a study of the increasing number of layers. The surface area corresponding to a given layer thickness can be determined from the surface area/surface pressure data recorded simultaneously with the X-ray data.

X-ray Reflectivity Measurements. The specular X-ray reflectivity (XR) data collection was performed with the liquid surface diffractometer installed at the undulator beamline BW1 in the synchrotron radiation research laboratory HASYLAB at DESY in Hamburg, Germany.[26,27] Using a NaI scintillation detector, the X-ray reflectivity was measured as a function of the vertical incidence angle, α_i, with the geometry, $\alpha_i = \alpha_f = \alpha$, where α_f is the vertical exit angle of the reflected X-rays. An X-ray wavelength of $\lambda = 1.304$ Å was used. XR data were collected as a function of the incidence angle, α_i, varied in the range 0.05−5°, corresponding to the range 0.01−0.85 Å^{-1} of the vertical scattering vector component $q_z = (4\pi/\lambda)\sin(\alpha)$.[28] The background scattering from, e.g., the subphase was measured at $2\theta_{xy} = 0.7°$ and subtracted from the signal measured at $2\theta_{xy} = 0$. The X-ray footprint area on the sample is inversely proportional to the incident angle of the X-rays (the footprint area is approximately 2×50 mm^2 for $\alpha_i \approx 0.1°$). The experimental setup is illustrated in Figure 2.

The sample cell for the X-ray scattering studies was a Teflon Langmuir film balance with an area of 440 cm^2 placed in an airtight aluminum container with Kapton windows. This sample cell allows variation of subphase temperature and area per molecule in the surface film. The surface pressure was measured with a Wilhelmy balance. A polished glass block immersed in the trough reduced the depth of the liquid phase to ca. 0.3 mm and thereby suppressed mechanically excited capillary waves. The liquid subphase was ultrapure water (18 MΩ cm) filtered in a Milli-Q apparatus (Millipore, Bedford, MA), unbuffered, at neutral pH and thermostated at $T = 22.0 \pm 0.2$ °C. X-ray experiments were performed in a He atmosphere saturated with water vapor and at constant surface pressure of the thin film.

Data Analysis. Specular X-ray reflectivity (XR) is required in order to gain information about the vertical structure of monomolecular layers or interfaces by measurement with a purely vertical scattering vector, q_z. The X-ray reflectivity data measured for CL-PMPhSi (Figure 3) have well-developed interferences, enabling a detailed analysis to extract from these "reciprocal space" XR data structural information in "direct space" for this complex structure thin polymer film consisting of several layers. The measured X-ray reflectivity, $R(q_z)$, is normalized by the Fresnel reflectivity, $R_F(q_z)$, calculated for a sharp air/water interface.[26] The extracted electron density profiles, $\rho(z)$, are normalized by the electron density

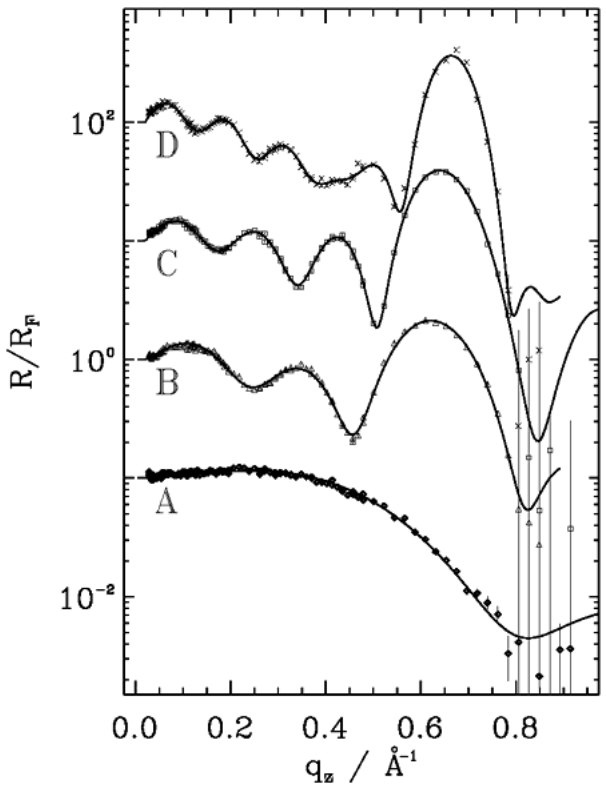

Figure 3. Synchrotron X-ray reflectivity measurements of CL-PMPhSi performed at different surface pressures: A ($\pi = 5.1$ mN/m), B ($\pi = 7.7$ mN/m), C ($\pi = 9.0$ mN/m), and D ($\pi = 11$ mN/m). The reflectivity $R(q_z)$ is normalized by the Fresnel reflectivity $R_F(q_z)$ and shown as a function of the vertical scattering vector, q_z. Observed data (points) and model-independent fits (solid lines) are displayed for clarity with an offset (A × 0.1; B × 1; C × 10; D × 100).

of the water subphase, $\rho_{water} = 0.334$ e/Å^3. The electron density profile, $\rho(z)$, is the laterally averaged structure, i.e., projected onto the z-axis, which is normal to the interface.

a. First Analysis. A vertically periodic homogeneous multilayer will give rise to a "Bragg peak" in the reflectivity curve, and from the peak position, q_z, the layer repeat distance, d, can be determined by $d = 2\pi/q_z$.[29] The full width at half-maximum (fwhm) of this peak gives information on the total layer thickness, $L \approx 0.88(2\pi)/\text{fwhm}(q_z)$.[16] In the present case where the sample consists of only a few layers on the water subphase, this method provides approximate structural information only. Bragg peaks in XR data were also observed for multilayer samples of *n*-alkanes assembled at the air/water interface.[29]

b. Second Analysis. Before attempting to build a detailed molecular model of these quite complex films, the application of a model-free data inversion strategy can be fruitful, e.g., the Pedersen−Hamley method.[30−32] In this method, the laterally averaged electron density, $\rho(z)$, is written as a smooth curve (in terms of cubic-spline functions); the X-ray reflectivity from such a model is calculated and refined to agree with the observed XR data by variation of the spline coefficients. A penalty on the deviations between neighboring spline coefficients provides a stabilizing constraint toward smooth $\rho(z)$ curves.[30−32] Transforming the assumed $\rho(z)$ to the corresponding normalized reflectivity curve by the so-called master formula[16]

$$R(q_z)/R_F(q_z) \approx \left|1/\rho_{subphase}\int (d\rho/dz)\exp(iq'_z z)\,dz\right|^2$$

inherently involves the assumption that the sample is laterally homogeneous or that the lateral scale of any inhomogeneity is less than several tens of nanometers. Only in this case is it valid to combine the variations into a laterally averaged $\rho(z)$ (*coherent* averaging).[16] The well-developed interferences in the XR data presented in this study seem to indicate that such *coherent* averaging is in order. If, conversely, the film consists of differing very large patches (micrometer size or larger), then the X-ray reflectivities must be calculated for each type of patch separately and averaged (i.e., an *incoherent* average).[16] The interferences will tend to get washed out, as illustrated by model calculations (see Figure 9) which show that, in a linear combination of reflectivity curves calculated for samples with different layer thickness, the modulations ("Kiessig fringes") are considerably reduced.

c. Third Analysis. Although classical "slab" models have sometimes been found to be inadequate for detailed modeling of high-resolution XR data,[33,34] the approach is useful here. The $\rho(z)$ profiles extracted by model-independent fittings can be further quantified by fitting classical slab models in real space to them. The resulting slab models, transformed by the *master formula*,[16] can then be fitted to the data in reciprocal space, allowing constraints like "all layers can be different" or "all polymer layers except the top layer must be equal". Each polymer layer is described by two slabs representing the organic moiety (methyl and phenyl) and the silicon- and oxygen-containing part. A thickness, L, and an electron density, ρ, parametrize each slab. One common smearing, σ, is applied to smoothen the artificial sharp interface between adjacent slabs.

3. Results

Surface Pressure−Area Isotherms. The $\pi-A$ isotherm data measured in this study are in agreement with the extensive work reported in the literature.[9] Figure 1 shows an isotherm for CL-PMPhSi measured at $T = 22$ °C during continuous compression where several steps and plateaus are visible approximately at 1/2, 1/3, ..., (1/n) monolayer area corresponding to a sample thickness of n layers.[9,35]

The area per monomer for CL-PMPhSi is previously estimated to 93 Å^2/monomer. In contrast to the cyclo-linear polysiloxanes with methyl substituents, in which all the steps in the isotherm data are well pronounced,[9,10,35,36] the second step for CL-PMPhSi is less pronounced at room temperature and above (see Figure 1). However, at lower temperatures the second step in the isotherm for CL-PMPhSi is clearly visible at an area per repeating unit of about 46 Å^2, corresponding to the transformation of the bilayer to a trilayer. Four XR experiments are performed as indicated by letters in Figure 1, corresponding approximately to a monomolecular layer (A) and a double (B), a triple (C), and four layer sample (D).

The surface pressure at the first plateau is close to the equilibrium spreading pressure, suggesting a monolayer−bilayer coexistence regime being close to the equilibrium state. At *constant area* relaxation of the surface pressure can be observed at the third or at higher plateaus, showing that the higher plateaus are nonequilibrium states.[36] However, thin films of CL-PMPhSi were found to be stable for hours, allowing several XR experiments to be performed at *constant pressures* on each sample (an XR investigation takes approximately 45 min; sample preparation and lining up the instrument also take some 30−60 min). Therefore, for practical purposes the thin films of CL-PMPhSi are considered to be stable structures. Notice that the isotherm data are measured during *continuous compression* of the sample whereas XR is measured at *constant surface pressure* of the sample.

X-ray Reflectivity Measurements. The observed X-ray reflectivity data and fitted curves for CL-PMPhSi are shown in Figure 3. The XR data, curve A, in Figure

Table 1. Bragg Peak Data from X-ray Reflectivity Measurements of CL-PMPhSi (See Figure 3)[a]

	q_z [Å^{-1}]	d [Å]	fwhm [Å^{-1}]	L_{tot} [Å]	L_{tot}/d
B	0.621	10.1	0.173	31.9	3.2
C	0.644	9.8	0.141	39.3	4.0
D	0.665	9.4	0.092	60.4	6.4

[a] The position of the "Bragg peak" in the reflectivity curve, q_z, provides information on the layer repeat distance, d, and the full width at half-maximum (fwhm) of this peak gives the total film thickness, L_{tot}. An estimate on the number of polymer layers in the thin film is calculated, L_{tot}/d.

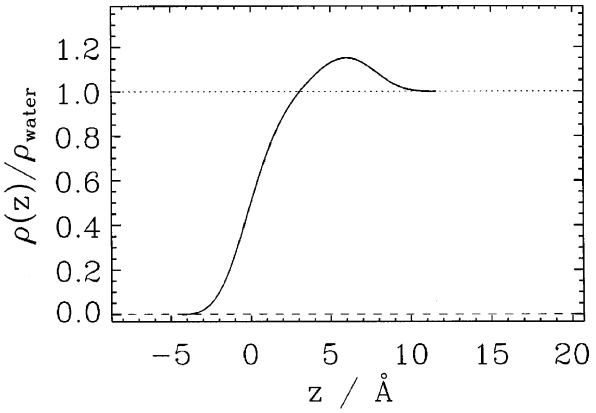

Figure 4. Electron density profile for CL-PMPhSi corresponding to the data (A) and fitted curve shown in Figure 3. The electron density, $\rho(z)$, is normalized by the electron density of the water subphase, $\rho_{water} = 0.334$ e/Å^3, and z is the surface normal.

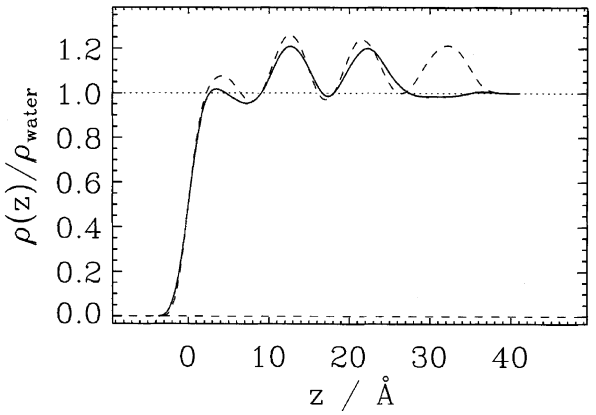

Figure 5. Electron density profiles for CL-PMPhSi at the air−water interface corresponding to the data and fitted curves shown in Figure 3, experiments B and C (dashed). The electron density, $\rho(z)$, is normalized by the electron density of the water subphase, $\rho_{water} = 0.334$ e/Å^3.

3 are measured for a monolayer sample according to the isotherm data. The increase in layer thickness for CL-PMPhSi on compression of the sample is clearly visible as an increase in the number of "Kiessig fringes" and as a narrowing of the "Bragg peak" (the large interference maximum) going from B to D in Figure 3. Approximate structural information, extracted from the full width at half-maximum and the position of the Bragg peaks, is given in Table 1.

As described above, a model-free method was applied to invert the XR data to electron density profiles $\rho(z)$ of the surfaces layers.[30−32] The electron density profile for a CL-PMPhSi monolayer is shown in Figure 4, whereas Figures 5 and 6 illustrate the electron density profiles for multilayer samples. Structural information extracted from Figures 4−6 is given in Table 2.

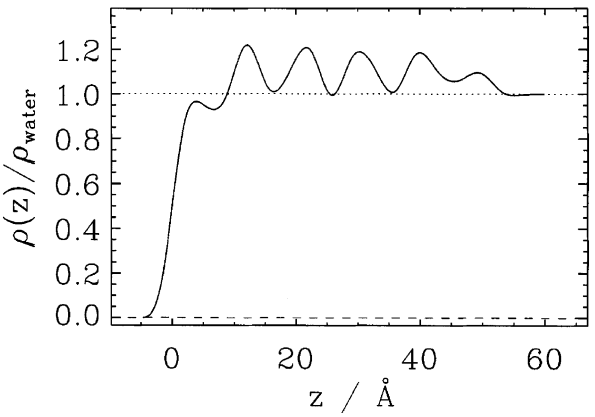

Figure 6. Electron density profiles for CL-PMPhSi corresponding to the data and fitted curves shown in Figure 3D. The electron density, $\rho(z)$, is normalized by the electron density of the water subphase, $\rho_{water} = 0.334$ e/Å^3.

The electron density profiles, $\rho(z)$, extracted by model independent fit can be further analyzed by fitting slab models in real space to them and applying the constraint: "all polymer layers can be different" or "all polymer layers except the top layer must be equal". These models where then refined to the observed XR data from experiments B and C. The slab model gives the same general shape of the electron density profiles as derived by the model-independent fit, although reducing the number of variables in the fit also slightly reduce the quality of the fit. The mean electron densities for the CL-PMPhSi thin films were extracted using slab models and are given in Table 2, including and excluding the top layer in the polymer film, denoted $\rho(z)_A$ and $\rho(z)_B$, respectively.

4. Discussion

Previous Structural Investigations. Development of physically reasonable molecular models corresponding to the electron density profiles extracted from XR data is not straightforward. Here we give a short summary of the available relevant structural data from other investigations.

The monomer of CL-PMPhSi could be crystallized, and a conventional X-ray diffraction structural investigation of the solid material was performed.[24] The crystal structure is shown in Figure 7, illustrating the layered nature of the solid monomer. The layer spacing is $d_{(1,-1,0)} = 9.53$ Å. It can be seen that there are layers of high electron density consisting of mainly silicium and oxygen atoms and low electron density regions containing mainly carbon and hydrogen. The short diagonal, $|a + b| = 13.16$ Å, is equal to the length of two monomers, so that the average length per monomer is 6.58 Å. Notice, however that in this structure half of the monomers are turned ca. 90° relative to the rest of the monomers; i.e., the Si/O rings are alternatingly oriented perpendicular to each other. It is useful to calculate the electron density for the bulk monomer in order to compare it with the polymer assembled at the air/water interface as a thin film. The mean electron density for the monomer can be estimated as $\rho_{aver} = F_{000}/V = 0.389$ e/Å^3 (corresponding to $\rho_{aver}/\rho_{water} = 1.168$) and is shown in Figure 7A. Electron density profiles were calculated for a hypothetical six-layer film of CL-PMPhSi using the bulk crystal structural data for the monomer, presenting each atom by a Gaussian charge distribution. Figure 7A show the results using different

Table 2. Structural Information from Electron Density Profiles Extracted by a Model Independent Method and Further Quantified Using Slab Models[a]

						no. of layers	
	π [mN/m]	$\langle L\rangle^b$ [Å]	$\langle\rho(z)_{max}\rangle$	$\langle\rho(z)_A\rangle$	$\langle\rho(z)_B\rangle$	n_A	n_B
A	5.1 ± 0.2	10.5	1.16 ± 0.05	1.11 ± 0.05		1	1
B	7.7 ± 0.2	10.3	1.22 ± 0.04	1.08 ± 0.04	1.10 ± 0.04	3	2
C	9.0 ± 0.2	10.3	1.24 ± 0.05	1.10 ± 0.05	1.11 ± 0.05	4	3
D	11.0 ± 0.2	9.7	1.20 ± 0.05			6	4

[a] A polymer layer in a thin film can be characterized by a thickness, L, and a maximum electron density, $\rho(z)_{max}$. The average layer thickness, $\langle L\rangle$, and average maximum electron density, $\langle\rho(z)_{max}\rangle$, are given for the well-defined polymer layers. The average electron density, $\langle\rho(z)_A\rangle$, for the thin film is calculated using slab models. The average electron density excluding the contribution from the top polymer layer is denoted $\langle\rho(z)_B\rangle$. The total number of polymer layers, n_A, can be compare to the number of well developed layers, n_B. [b] For experiments B and C the top layer is not included in the calculation of the average layer thickness, and for experiment D the top and bottom layers are not included.

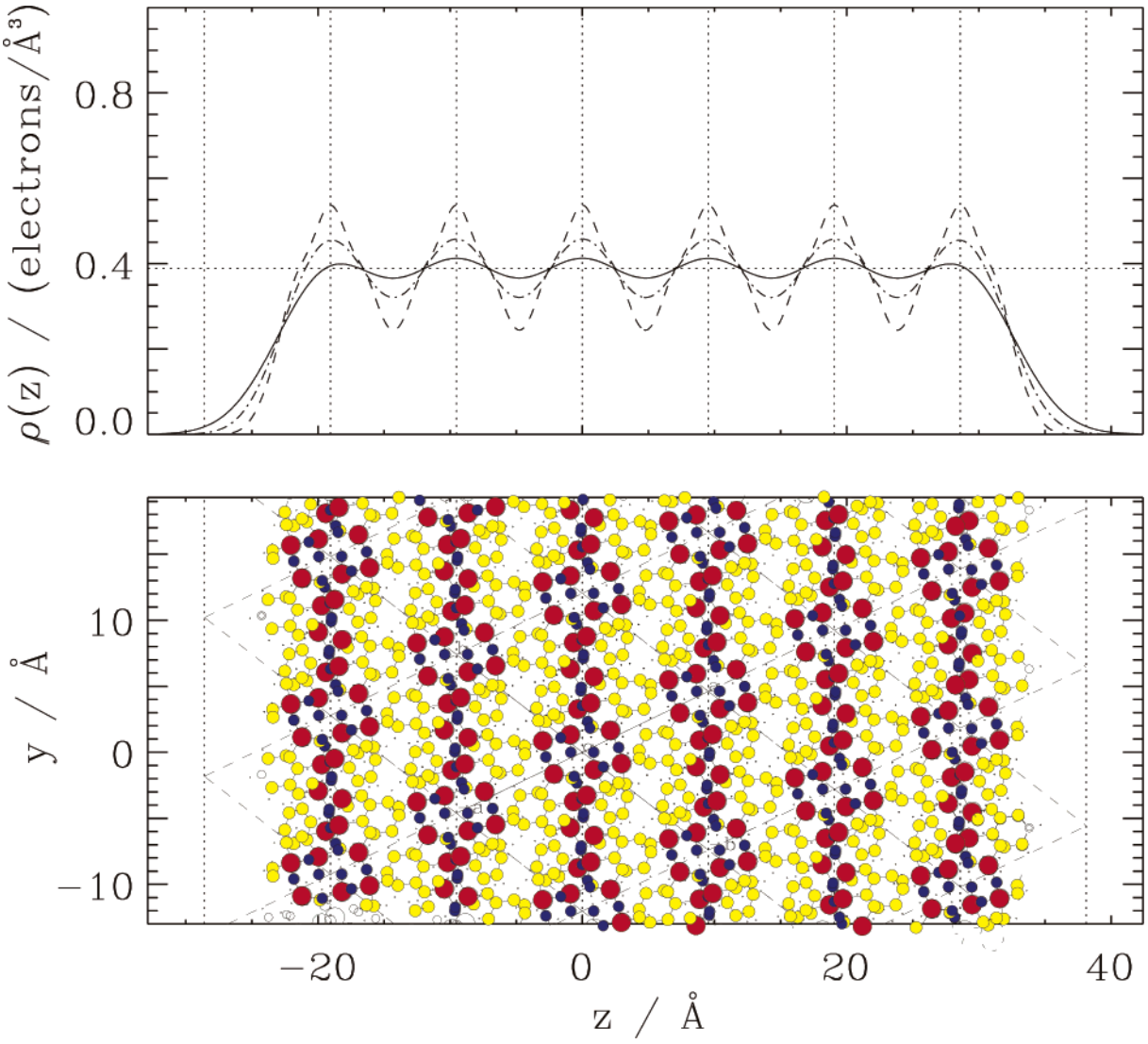

Figure 7. (A, top) Electron density profiles, $\rho(z)$, for a six-layer-thick film of CL-PMPhSi were calculated using the atomic coordinates from the bulk crystallized monomer representing each atom by an Gaussian electron distribution. The $\rho(z)$ profile was smeared by $\sigma = 1$ (dashed), 2 (dash−dotted), and 3 Å (full line), σ representing the (rms) surface roughness from capillary waves. The mean electron density for the bulk monomer is shown as a dotted line, $\rho_{aver} = F_{000}/V = 0.389$ e/Å^3 ($\rho_{aver}/\rho_{water} = 1.168$). (B, bottom) Crystal structure of the bulk CL-PMPhSi monomer shown as an *a*,*b*-projection (the *c*-axis out of the paper). The atomic radii are proportional to the atomic number. Notice that the rings formed by silicium (red) and oxygen (blue) are alternatingly oriented perpendicular to each other. Carbon is yellow, and hydrogen is shown as small size black circles.

smearing, $1 < \sigma < 3$ Å (rms), and with the (1,−1,0) planes parallel to the water surface. In Figure 7 the water subphase is not included in the calculations.

A trimer segment of transtactic cyclolinear poly(methylphenylsiloxane), CL-PMPhSi, was investigated by molecular modeling including a slab of water molecules to simulate the effect of the air−water interface.[35] The plane of the siloxane ring was found to be parallel to the subphase with half of the phenyl groups above and the rest below the Si/O ring. The trimer was 28 Å long and 10 Å wide, and the thickness of the monolayer was calculated to be 10.9 Å.

Structural Model for Thin Films of CL-PMPhSi at the Air/Water Interface. The macroscopic mea-

surements of isotherm data (see Figure 1) suggest a stepwise collapse with a *successively* increasing layer thickness of the thin film of CL-PMPhSi. The extracted electron density profiles from in situ X-ray reflectivity measurements for multilayer samples of CL-PMPhSi clearly show alternating regions with low and high electron density in the direction parallel to the surface normal, implying that these multilayer samples have distinct layers of polymers (see Figures 5 and 6). Therefore, we infer that the multilayer sample contains distinct sublayers with mainly silicon and oxygen atoms while the other sublayers contain mainly the organic substitutes (methyl and phenyl). It is suggested from molecular modeling of the CL-PMPhSi trimer and from the bulk crystalline structure of the monomer that half of the phenyls are above and half below the Si/O rings.[24,35] According to these observations, the polymers in a multilayer are possibly arranged as follows: subphase [water]−first polymer [organic substitutes−Si/O framework−organic substitutes]−second polymer [organic substitutes−Si/O framework−organic substitutes]− etc. The subphase water and the organic material (methyl and phenyl) have similar electron density, and the exact boundary between subphase and the thin film is not clearly visible. It was found that CL-PMPhSi has a contact angle of 89 ± 1° (measured for CL-PMPhSi deposited on mica), reflecting the delicate balance between the hydrophobic and hydrophilic interactions.[35]

We observe maximum normalized electron densities of ca. 1.25 and minimum a little less than 1.0 (see Figures 5 and 6), and the observed polymer layer thickness is ca. 9−10 Å for CL-PMPhSi. These results for the thin film resemble the data from the bulk monomer despite possible structural differences as shown in Figure 7B. The best fit smearing for the comparison of calculated (Figure 7) and observed (Figures 4−6) electron density profiles was $\sigma = 2.7$ Å, as shown in Figure 8. There is good correspondence between the model calculations (bulk monomer) and the observations (XR) measured in situ at the air/water interface. The total number of polymer layers in each thin film can easily be counted as well as the well-developed layers, denoted n_A and n_B, respectively, in Table 2. The number of well-developed layers, n_B, correspond to the expected layer thickness from the isotherm measurements, whereas n_A is in accordance with the first analysis shown in Table 1. The polymers in a multilayer of CL-PMPhSi might have a structure akin to Figure 7B, with phenyl rings on both sides of the siloxane rings but, maybe, with all siloxane rings in a polymer in the same plane parallel to the subphase in accordance with MD simulations.[35] The structural motif of Figure 7B would then have the subphase parallel to the (1,−1,0) planes.

It might have been speculated that the sample in the relatively large X-ray footprint area (up to ca. 2 × 50 mm^2) would consist of domains with different numbers of polymer layers, giving rise to the apparent lower electron density of the top layer in a multilayer sample visible in the $\rho(z)$ profiles (see Figures 5 and 6). Such a sample would give rise to average structural information obtained from the XR investigations, albeit with the caveats discussed above (i.e., coherent *vs* incoherent averaging).[16] However, linear combinations of calculated XR data for samples with n and $n + 1$ layers result in too low contrast of the modulations ("Kiessig fringes") compared to the observed data (see Figure 9), revealing

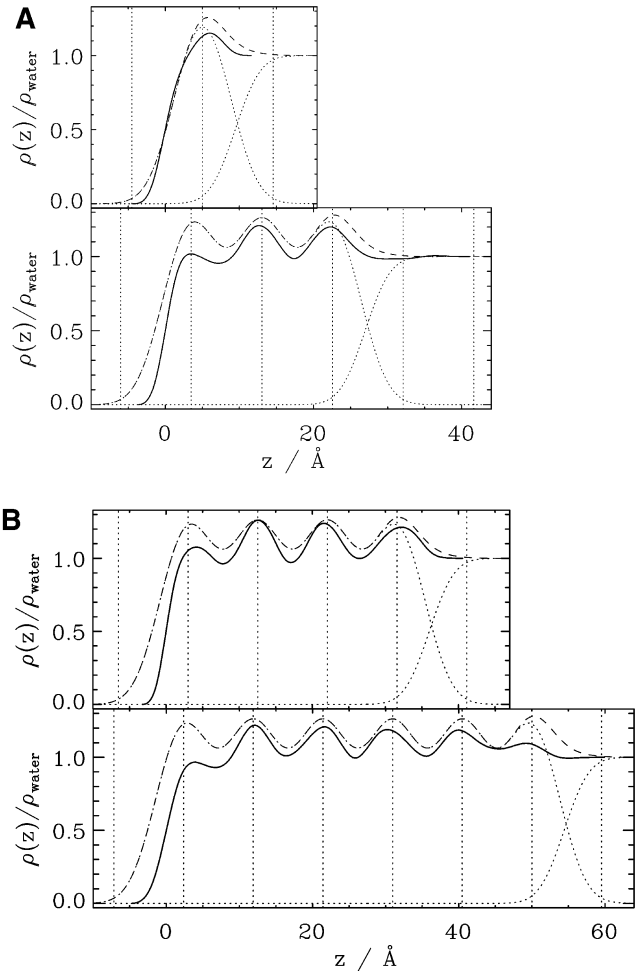

Figure 8. Calculated electron density profiles, $\rho(z)$, for one- and three-layer-thick films of CL-PMPhSi floating at the air−water interface and for four and six layers is shown as dashed lines in (A) and (B), respectively. The electron density for the interface (dashed) is calculated as the sum of the electron density of the thin film (dotted) and the water subphase (dotted) smeared by $\sigma = 2.7$ Å. The observed electron density profiles for the interface (full lines) from experiments A and B (see Figures 4 and 5) are shown in (A) and from experiment C and D (see Figures 5 and 6) in (B).

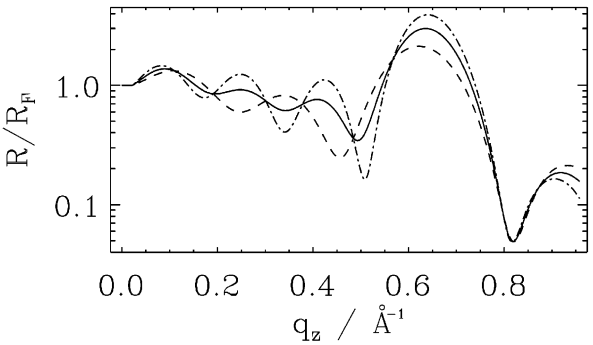

Figure 9. A 50:50 linear combination (full line) of calculated X-ray reflectivity data corresponding to samples with two (dashed) and three layers (dash−dotted). The "Kiessig fringes" in the averaged reflectivity curve tend to be washed out.

that each of the investigated samples has a well-defined number of layers and that *domains* with different layer thickness are not observed with the X-ray reflectivity measurements so that coherent XR averaging occurs.[16] AFM performed on CL-PMPhSi transferred to solid support showed relatively homogeneous samples with

a relatively low number of defects,[35] in accordance with the present XR investigation indicating no inhomogenities. Notice here that XR probes less than 2×50 mm^2 out of a total sample area of 100−400 cm^2 and is performed in situ on the liquid interface.

The samples have a controllable layer thickness within at least 1−6 polymer layers, i.e., ca. 1−6 nm, and any lateral inhomogeneity appears to be of lateral short scale (local defects). Furthermore, any lateral inhomogeneity is less than some tens of nanometers. The polymers have only weak interactions between the chain termini, and inhomogeneities can possibly arise where polymers are not juxtaposed. Perpendicular to the polymer chain there may be relatively strong $\pi-\pi$ interactions between phenyls. This might explain the high degree of structural order in the multilayers with polymers lying flat and straight on the water surface and with the ability to self-organize after a change in surface area of the sample.

The silicon and oxygen rich slabs in CL-PMPhSi multilayers show a tendency for increasing maximum electron density accompanied by decreasing layer thickness as the number of layers increase and away from the subphase, as illustrated in Figures 5 and 6. This suggests a more dense packing of the polymers in the thin film and a more loose packing at the film surfaces. Furthermore, the XR data suggest that there might exist structural differences in the molecular packing of polymers in a monolayer and the top layer of a multilayer compared to polymers in the bulk of a multilayer. This can be seen from the less pronounced maximum in the electron density for the monolayer (Figure 4) and the maximum electron density given in Table 2. Polymers in a monolayer and the top layer of a multilayer possibly have a slightly different conformation optimizing the hydrophobic and hydrophilic intermolecular interactions between polymers and with the subphase.

5. Conclusion

The investigated CL-PMPhSi polymer reveals an interesting example of "bottom-up" self-assembly of polymer nanostructures. Manipulation of the surface pressure leads to ordered architectures with any lateral inhomogeneity less than some tens of nanometers. Therefore, we conclude that the samples have a very uniform layer thickness and that there is a significant degree of structural order in the packing of these polymers as multilayers, i.e., two-dimensional structural order in a direction perpendicular to the polymer axis in and out of plane, as the individual polymers are not necessarily in registry at the termini. Surprisingly, there is very little interdigitation between adjacent polymer layers, which would lead to a larger smearing of the electron density. This is probably due to a strong incompatibility of the different molecular entities, i.e., hydrophobic/hydrophilic interactions. The observed results suggest that there is a specific mechanism responsible for the multilayer formation, which relatively fast reaches equilibrium short time after a change in surface pressure as the investigated samples have a well-defined layer thickness, and the samples do not consist of domains with different thickness. Furthermore, the samples are stable at least for several hours. The interplay between hydrophobic and hydrophilic interactions is probably important for the assembly of the monomolecular layer whereas intermolecular interactions between phenyl rings possibly dominate the self-organization of multilayers, resulting in a high degree of structural order. We propose that these materials can serve as templates for a variety of different applications and devices, e.g. by addition of side chains on some of the monomers for further functionalization, and that this study opens new prospects within polymer film engineering.

Acknowledgment. We are grateful to Prof. J. Skov Pedersen, Aarhus University, Denmark, for helpful discussions and for a copy of his program, LSQREFL. This work is part of the INTAS and RFBR (Russian Foundation for Basic Research) research programs and was supported under Grants INTAS 97-485 and RFBR 99-03-33351. Further, we are grateful to the Danish National Research Council under the program DANSYNC for financial support and to HASYLAB at DESY, Hamburg, Germany, and the European Community (Contract HPRI-CT-1999-00040) for beam time. Yu.K.G. and J.R.-G. thank the Alexander von Humboldt Foundation for a Research Award. J.R.-G. also thanks CONACYT for support. T.R.J. thanks the Danish National Research Council for a Steno Stipend.

References and Notes

(1) Lehn, J.-M. *Science* **2002**, *295*, 2400−2403.
(2) Ikkala, O.; Brinke, G. T. *Science* **2002**, *295*, 2407−2409.
(3) Förster, S.; Plantenberg, T. *Angew. Chem.* **2002**, *41*, 688−714.
(4) Lewis, H. G. P.; Edell, D. J.; Gleason, K. K. *Chem. Mater.* **2000**, *12*, 3488−3494.
(5) Ouyang, M.; Yuan, C.; Muisener, R. J.; Boulares, A.; Koberstein, J. T. *Chem. Mater.* **2000**, *12*, 1591−1596.
(6) Yilgör, I.; McGrath, J. E. *Adv. Polym. Sci.* **1988**, *86*, 1.
(7) Kaganer, V. M.; Möhwald, H.; Dutta, P. *Rev. Mod. Phys.* **1999**, *71*, 779−819.
(8) Gaines, G. L. *Insoluble Monolayers at Liquid−Gas Interfaces;* Interscience: New York, 1966.
(9) Buzin, A. I.; Sautter, E.; Godovsky, Yu. K.; Makarova, N. N.; Pechhold, W.; *Colloid Polym. Sci.* **1998**, *276*, 1078−1087.
(10) Makarova, N. N.; Godovsky, Yu. K. *Prog. Polym. Sci.* **1997**, *22*, 1001−1052.
(11) Godovsky, Yu. K.; Makarova, N. N.; Matukhina, E. V. Mesophase behavior and structure of mesophases in cyclolinear polyorganosiloxanes. In *ACS Symposium Series No. 729*; Clarson, S., Ed.; American Chemical Society: Washington, DC, 2000; Chapter 6. See also references therein.
(12) Ibn-Elhaj, M.; Riegler, H.; Möhwald, H. *J. Phys. I* **1996**, *6*, 969−980.
(13) Mann, E. K.; Hénon, S.; Langevin, D.; Meunier, J. *J. Phys. II* **1992**, *2*, 1683−1704.
(14) Godovsky, Yu. K.; Papkov, V. S.; Magonov, S. N. *Macromolecules* **2001**, *34*, 976−990.
(15) Tidswell, I. M.; Rabedeau, T. A.; Pershan, P. S.; Folkers, J. P.; Baker, M. V.; Whitesides, G. M. *Phys. Rev. B* **1991**, *44*, 10869−10879.
(16) Jensen, T. R.; Kjaer, K. In *Novel Methods to Study Interfacial Layers, Studies in Interface Science*; Miller, R., Ed.; Elsevier Sciences B.V.: Amsterdam, 2001; Vol. 11, pp 205−255.
(17) Weissbuch, I.; Popovitz-Biro, R.; Lahav, M.; Leiserowitz, L.; Kjær, K.; Als-Nielsen, J. *Adv. Chem. Phys.* **1997**, *102*, 39−120.
(18) Reitzel, N.; Kjaer, K.; Howes, P. B.; Jensen, T. R.; Fechtenkötter, A.; Brand, J. D.; Ito, S.; Müllen, K.; Bjørnholm, T. *Chem.−Eur. J.* **2001**, *7*, 4894−4901.
(19) Buller, R.; Cohen, H.; Jensen, T. R.; Kjaer, K.; Lahav, M.; Leiserowitz, L. *J. Phys. Chem. B* **2001**, *105*, 11447−11455.
(20) Makarova, N. N.; Lavrukhin, B. D. *Izv. Akad. Nauk SSR, Ser. Khim.* **1986**, 652−659.
(21) Godovsky, Yu. K.; Makarova, N. N.; Kuzmin, N. N. *Macromol. Chem., Macromol. Symp.* **1989**, *26*, 91−109.
(22) Makarova, N. N.; Petrova, I. M.; Godovsky, Yu. K.; Zhdanov, A. A. *Patent (Russia)* **1993**, N1126579.
(23) Mamaeva, I. I.; Petrova, I. M.; Makarova, N. N.; Tverdoxlebova, I. I.; Pavlova, S. A. *Vysokomol. Soed.* **1987**, *29A*, 1507−1511.

(24) Polistshuk, A. P.; Makarova, N. N.; Astapova, T. V. *Krystallografiya* **2002**, *47*, 863−868.
(25) Makarova, N. N.; Godovsky, Yu. K.; Lavrukin, B. D. *J. Polym. Sci., Part A* **1995**, *37*, 225−241.
(26) Als-Nielsen, J.; Jacquemain, D.; Kjaer, K.; Leveiller, F.; Lahav, M.; Leiserowitz, L. *Phys. Rep.* **1994**, *246*, 251−313.
(27) Frahm, R.; Weigelt, J.; Meyer, G.; Materlik, G. *Rev. Sci. Instrum*. **1995**, *66*, 1677−1680.
(28) Kjaer, K. *Physica B* **1994**, *198*, 100−109.
(29) Weinbach, S. P.; Weissbuch, I.; Kjaer, K.; Bouwman, W. G.; Als-Nielsen, J.; Lahav, M.; Leiserowitz, L. *Adv. Mater*. **1995**, *10*, 857−862.
(30) Pedersen, J. S. *J. Appl. Crystallogr.* **1992**, *25*, 129−145.
(31) Hamley, I. W.; Pedersen, J. S. *J. Appl. Crystallogr*. **1994**, *27*, 29−35.
(32) Pedersen, J. S.; Hamley, I. W. *J. Appl. Crystallogr*. **1994**, *27*, 36−49.
(33) Schalke, M.; Lösche, M. *Adv. Colloid Interface Sci*. **2000**, *88*, 243−274.
(34) Schalke, M.; Krüger, P.; Weygand, M.; Lösche, M. *Biochim. Biophys. Acta* **2000**, *1464*, 113−126.
(35) Buzin, A. I.; Godovsky, Yu. K.; Makarova, N. N.; Fang, J.; Wang, X.; Knobler, C. M. *J. Phys. Chem. B* **1999**, *103*, 11372−11381.
(36) Buzin, A. I.; Sautter, E.; Godovsky, Yu. K.; Makarova, N. N.; Pechhold, W. *Russ. Polym. Sci.* **1998**, *A40*, 443−447.

MA034473C